Characterization of the genetic architecture underlying eye size variation within *Drosophila melanogaster* and *Drosophila simulans*

Pedro Gaspar[*], Saad Arif[*], Lauren Sumner-Rooney[†], Maike Kittelmann[*], David L. Stern[††], Maria D. S. Nunes[*,1] and Alistair P. McGregor[*,1]

* Department of Biological and Medical Sciences, Oxford Brookes University, Gipsy Lane, Oxford, OX3 0BP, UK

[†] Oxford University Museum of Natural History, Parks Road, Oxford OX1 3PW, UK

[††] Janelia Research Campus, Howard Hughes Medical Institute, Ashburn, VA 20147, USA

[1]Corresponding authors:

E-mail: msantos-nunes@brookes.ac.uk, amcgregor@brookes.ac.uk

Tel: +44 (0)1865 484191

Fax: +44 (0)1865483242

Running title: Evolution of *Drosophila* eye size

Key words: *Drosophila,* evolution, development, organ size, eye, head capsule

Abstract

Insect compound eyes exhibit striking variation in size caused by changes in the number and/or diameter of ommatidia. These changes can affect the contrast sensitivity and visual acuity of the vision of these animals thereby facilitating adaptations to different lifestyles and habitats. However, the genetic basis of changes in insect eye size is poorly understood. Here, we describe extensive eye size variation within and between species of the *Drosophila melanogaster* species subgroup, which offers an opportunity to address both the genetic and developmental bases of size variation. We mapped quantitative trait loci (QTL) in *D. melanogaster* and *D. simulans* underlying intra-specific variation in eye size, mainly caused by differences in ommatidia number, and in inter-ocular distance. We found that in both cases QTL appear to be largely overlapping for both of these head traits, suggesting that the same loci may expand eye size at the expense of face cuticle and vice versa. Furthermore, although these traits have low heritability and are polygenic, we were able to identify some QTL, whose location estimates overlap between these two species. This may indicate some common genetic basis for eye size variation between these two species. However, we observed differences in eye fate commitment between strains of *D. melanogaster* and *D. simulans* suggesting different developmental mechanisms contribute to eye size variation in these species. Considering the results of previous studies, our findings suggest that the gene regulatory network that specifies eye size has evolved at multiple nodes to give rise to natural variation in this trait within and among species.

Introduction

Animal sensory organs show great morphological variation within and between species. For example, dipteran compounds eyes display remarkable diversity in shape and can differ dramatically in size as a result of differences in ommatidia number and size (Norry *et al.* 2000; Hämmerle and Ferrús 2003; Domínguez and Casares 2005; Sukontason *et al.* 2008; Land 2009; Posnien *et al.* 2012; Arif *et al.* 2013; Hilbrant *et al.* 2014; Ramaekers *et al.* 2018). However, little is known about the genetic loci underlying this variation and the evolutionary forces that shape and maintain this diversity.

Variation in ommatidia number and size has important implications for vision. Where ommatidial length is constant, higher numbers of ommatidia can increase acuity, while larger ommatidia may reduce acuity by increasing inter-ommatidial angles but improve contrast sensitivity (Land 2002; Theobald *et al.* 2010; Land and Nilsson 2012).

The size of insect compound eyes also appears to be constrained by negative correlation with the relative size of the overall head capsule (Posnien *et al.* 2012). In this case, negative size correlations arise through subdivision of a developmental precursor, the eye-antennal imaginal disc, where eye tissue appears to differentiate at the expense of head capsule tissue (Garcia-Bellido *et al.* 1973; Crick and Lawrence 1975; Riska 1986; Domínguez and Casares 2005). This may be of considerable importance in morphological evolution because negatively correlated traits can evolve in opposite directions, resulting in a substantial change in relative size and shape (Norry *et al.* 2000; Posnien *et al.* 2012; Arif *et al.* 2013). Drastic changes in head tissues may be driven by sexual selection, such as in the cases of hypercephaly in stalked-eyed flies (Wilkinson and Reillo 1994; Cotton *et al.* 2010) and the sister species *Drosophila heternoneura* and *D. sylvestris* (Spieth 1981; Kaneshiro and Boake 1987). However, although some progress has been made in mapping QTL underlying these differences, the causative genes remain unknown (Templeton 1977; Val 1977; Burkhardt and de la Motte 1988; Hingle *et al.* 2001; Cotton *et*

al. 2014).

The *Drosophila melanogaster* species subgroup exhibits substantial variation in eye size caused by differences in the diameter and/or number of ommatidia (Norry *et al.* 2000; Hämmerle and Ferrús 2003; Posnien *et al.* 2012; Arif *et al.* 2013; Hilbrant *et al.* 2014; Ramaekers *et al.* 2018). QTL mapping has revealed that variation in eye size between *D. mauritiana* and *D. simulans,* and within *D. melanogaster* is polygenic (Arif *et al.* 2013; Norry and Gomez 2017). Strains of *D. mauritiana* have larger eyes than either *D. melanogaster* or *D. simulans*, which mainly results from a difference in ommatidial diameter caused by a X-linked locus/loci of large effect (Posnien *et al.* 2012; Arif *et al.* 2013). In this case, QTL mapping showed eye and face width (inter-ocular distance) are influenced by non□overlapping loci (Arif *et al.* 2013). In contrast, mapping using *D. melanogaster* recombinant inbred lines suggested the occurrence of both distinct and common genetic bases for eye and head capsule variation (Norry and Gomez 2017). Additionally, a genome-wide association study in *D. melanogaster* found an association between six SNPs upstream of the *kek1* gene and female inter-ocular distance (Vonesch *et al.* 2016). More recently, a polymorphism in the 3rd intron of *eyeless* (*ey*) has been associated with differences in eye size between *D. melanogaster* strains and between this species and *D. pseudoobscura* (Ramaekers *et al.* 2018). However, the polygenic basis of eye size differences within and between species suggests that other genetic and developmental changes likely also contribute to this variation.

In this study we further explore variation in eye and head capsule morphology in *D. melanogaster* and *D. simulans*, and investigate and compare the genetic and developmental bases for intra-specific differences in eye size in these species. This provides new insights into the genetic architecture and developmental mechanisms underlying eye size variation and the trade-off with head capsule size within and between species.

Materials and Methods

Fly strains and husbandry

Multiple strains of the sister species *D. melanogaster*, *D. simulans*, *D. mauritiana* and *D. sechellia* were used in this study, including strains from the ancestral range and other populations of *D. melanogaster* and *D. simulans* (Table S1). Flies were maintained on a standard cornmeal diet at 25°C under a 12:12 hour dark/light cycle. For experiments, flies were reared at a density of fewer than 30 larvae per vial.

Phenotypic measurements

All parental strains were imaged from frontal or lateral views of the head and the *D. melanogaster* QTL mapping population was imaged from frontal head views, captured by a Zeiss AxioZoom.V16 (7x…112x) microscope mounted with an objective Apo Z 1.5x/0.37 FWD 30mm and Axiocam 506 colour (D) camera. For the *D. simulans* mapping population, frontal images of the head were taken using a Leica M205 stereomicroscope and a DFC300 Camera. Eye area was measured as the sum of outlined eye taken from frontal images of the head, as described in Posnien *et al.* 2012, and the width of the cuticle between the eyes (face width/inter-ocular distance) was measured at the height of the orbital bristles just above the antennae. All frontal images were further annotated with a combination of 45 landmarks and semi-landmarks as described in Posnien *et al.* 2012 (Fig. 2C). The landmarks coordinates were then subjected to a Generalized Procrustes Analysis (GPA) to standardize for size, position and orientation. We analyzed variation in head shape using Principal Component Analysis (PCA) of the GPA aligned configurations of head shapes and visualized these differences using thin-plate spline (TPS) deformation grids. All morphometric analysis was performed using the ‘geomorph’ R package (Adams and Otárola-Castillo 2013). The length of the middle (T2) or the most posterior (T3) leg tibias were measured as a proxy for overall body size. To determine ommatidia number,

lateral images of the head were segmented using the Valleys algorithm for identification of dark lines (ommatidia boundaries) against a bright background (pigmented facets) in the Zeiss AxioVision 4 software (Fig. S1). After applying a gaussian blur (sigma=1) segmented images were converted into binary format using an autothreshold via the IsoData algorithm and ommatidia were counted using the Analyse Particles plugin in the Fiji image analysis software (Fig. S1). To determine ommatidial diameter, lens diameters were measured from 10 central ommatidia in each lateral head image (Posnien *et al.* 2012) (Fig. S1). All linear measurements and landmark annotations were performed with the Fiji image analysis software. Statistical analysis of species, sex and strain differences in eye area, inter-ocular distance and tibia length within the *D. melanogaster* species subgroup survey was done using ANOVA and individual differences were tested using the Tukey multiple comparisons test (see Table S3 for sample sizes). Ommatidia number differences or ommatidial diameter differences were assessed using t-tests.

X-ray imaging

Fly heads were dissected under CO_2 and placed into fixative (2% paraformaldehyde and 2.5% glutaraldehyde in 0.1 M sodium cacodylate buffer) for 1 hour, shaking gently at room temperature and then for a further 15 hours at 4°C. Samples were then washed in water and stained with 1% osmium tetroxide (aq) for 48 hours at 4°C. After thorough washing in water, samples were dehydrated in a series of ethanol concentrations up to 100% EtOH over two days. Infiltration with 812 epoxy resin (Taab) was done over 3 days. Finally, samples were embedded in embedding moulds and polymerised for 24 hours at 70°C. Resin blocks with fly heads were mounted on brass stubs for synchrotron radiation X-ray tomography (SRXT) and scanned at the TOMCAT beamline (Swiss Light Source, Paul Scherrer Institute, Villigen, Switzerland). Samples were scanned with a monochromatic beam at an energy of 18 keV, using a combined magnification of 20x (effective isotropic

pixel size 325 nm). Scans comprised 1501 projections, rotating through a total of 180°, with an exposure time of 180 ms. Propagation distance between the sample and the scintillator was 25 mm. Scans were reconstructed into TIFF stacks and Paganin filtered (Delta = $1e^{-7}$, Beta = $1e^{-8}$) at TOMCAT using in-house software. IMOD Software package (Kremer et al., 1996) was used to generate mrc stacks from reconstructed tomogram TIFF files. Stacks were binned by 2 in X and Y to reduce file size for 3D segmentation in Amira (Thermo Fisher Scientific). Ommatidial facets and head structures were segmented by masking the structure of interest and applying the threshold tool within that mask. Ommatidial diameter was measured with the 3D line measurement tool on the segmented eye from the dorsal to ventral side of the facets.

Genetic markers

DNA was extracted from adult fly abdomens. Genotyping for the *D. melanogaster* QTL mapping population was performed with restriction fragment length polymorphisms (RFLP) at 42 loci regularly spaced across all four chromosomes (Table S2). The mean distance between consecutive markers was 6.64 cM, with the maximum distance between markers being 15.3 cM. *D. melanogaster* genomes were obtained from the Drosophila Genome Nexus and aligned to the *D. melanogaster* reference genome BDGP release 5 (Pool *et al.* 2012) (SRP005599, http://www.johnpool.net/genomes.html). Genotyping for the *D. simulans* mapping population was performed with multiplexed shotgun genotyping (MSG) (Andolfatto *et al.* 2011), resulting in 6152 SNPs for the backcross to the Tana10 strain and 8115 SNPs for the backcross to the Zom4 strain (Files S1-S6). Parental genomes were generated by updating the *D. simulans* r2.0.1 genome (http://www.flybase.org/static_pages/feature/previous/articles/2015_02/Dsim_r2.01.html) with HiSeq reads from each strain (these genomes are available on request). Genotypes were estimated using the MSG software

(https://github.com/YourePrettyGood/msg/tree/dev).

QTL mapping

To generate the *D. simulans* QTL mapping population, *D. simulans* Zom4 females were mated to *D. simulans* Tana10 males. F1 virgin females were then backcrossed to either Zom4 males or Tana10 males as density controlled replicates of 5 females crossed to 5 males. The heads of 192 females and 192 males from each backcross progeny (totaling 384 individuals) were phenotyped and their bodies were processed into a single MSG library for each backcross (Files S1-S6, Fig. S2). To generate the *D. melanogaster* QTL mapping population, *D. melanogaster* ZI373 females were mated to *D. melanogaster* RG13N males, or reciprocally. F1 progeny from each reciprocal parental cross were mated to siblings as density-controlled replicates of 5 females crossed to 5 males. The heads of 48 F2 females and 48 F2 males from each cross direction (totaling 192 individuals) were phenotyped and their bodies processed for genotyping with RFLPs (File S7, Fig. S2).

QTL mapping and statistical analyses

For the *D. simulans* genotype dataset, posterior probabilities of ancestry were thinned and imported into R/qtl using custom scripts (http://www.github.com/dstern/pull_thin, http://www.github.com/dstern/read_cross_msg). To determine QTL locations for both *D. melanogaster* and *D. simulans*, we performed genome scans with a single QTL model using R/qtl to perform standard interval mapping with Haley-Knott regression (Haley and Knott 1992; Broman *et al.* 2003). Genome-wide statistical significance thresholds (0.05%) were determined for each phenotype using 1000 permutations. For both the *D. melanogaster* and *D. simulans* QTL analyses we filtered any individuals with > 10% missing data and any markers with > 10% missing data. Additionally, for *D. simulans,* we only retained markers that were at least 2.5 kilobases (kb) apart for computational

efficiency. To identify QTLs in *D. melanogaster* and *D. simulans* we used the native R/qtl forward search/backward elimination search algorithm (as implemented using the 'stepwiseqtl' function) followed by a final scan for any additional QTL, after accounting for those discovered in the previous step. We used the lengths of tibias T2 and T3 (as proxies for body size) and sex as covariates, to account for size and dimorphism, while searching for QTLs associated with eye size and inter-ocular distance. Only sex was used a covariate while searching for QTL associated with lengths of tibias T2 and T3. We calculated 2□LOD support intervals for all significant QTL and tested for pair□wise interactions between all significant QTL by fitting full linear models in an ANOVA framework (F□tests, type III sum of squares), with all significant QTL and a proxy for body size as fixed effects. Furthermore, we estimated additive allelic effects of all significant QTL in three ways for autosomes: (1) the additive effect as half the standardized difference between the means of the homozygotes (ZI373/ZI373, RG13N/RG13N, Zom4/Zom4, Tana10/Tana10), (2) the dominant effect (only for the F2 cross) as the standardized difference between the mean of the heterozygotes (ZI373/RG13N) and the average of the homozygote means (and ZI373/ZI373, RG13N/RG13N), (3) the percentage of phenotypic variation accounted for by the significant QTL in the mapping population (variance explained).

Immunohistochemistry

Imaginal discs were dissected in phosphate buffer saline (PBS) and fixed in 4 % (v/v) formaldehyde in PBS for 30 min. Following three washes with PBS, samples were permeabilised in 0.3% (v/v) Triton X-100 in PBS (PBST), then blocked in 5% normal goat serum (Sigma) in PBST before incubation with primary antibodies in this solution overnight. Secondary antibodies were incubated with samples for 2 hours at 4ºC before mounting in 80% (v/v) glycerol in PBS. Primary antibodies used were: mouse anti-Eyes

absent (Eya) (1:10, DCAD2, Developmental Studies Hybridoma Bank [DSHB]) and rat anti-Elav (1:200, 7E8A10, DSHB). Secondary antibodies used were goat anti-rat or anti-mouse, Alexa 488 and goat anti-rat or anti-mouse Alexa 647 (Molecular Probes), at 1:500 dilutions. Nuclear staining was performed using DAPI (Roche). Fluorescence images were acquired using a Zeiss LSM880 confocal microscope. Tissue surface area was measured across apical and basal optical sections using the outline tools of the Fiji image analysis software.

Results

Variation in eye size within and between Drosophila *species*

It was previously shown that the eyes of a limited number of strains of species in the *D. melanogaster* complex show substantial intra- and interspecific variation (Norry *et al.* 2000; Hämmerle and Ferrús 2003; Posnien *et al.* 2012; Arif *et al.* 2013; Hilbrant *et al.* 2014; Ramaekers *et al.* 2018). To widen the survey of this variation, we measured the eye size, inter-ocular distance and tibia lengths of strains of *D. melanogaster* and *D. simulans* from around the world including from the ancestral range, as well as strains of *D. mauritiana* and *D. sechellia* (Fig. 1, Fig S3, Table S3). We detected significant differences in eye area and inter-ocular distance between species, sexes and between strains of the same species (Fig. 1, Fig. S3, Table S3). In agreement with previous observations, the eyes of females are generally larger than those of males, although the degree eye size sexual dimorphism varies widely across strains (Fig. 1, Tables S3, S4). Nevertheless, we did not detect a significant species by sex interaction for eye area, inter-ocular distance or tibia length variation in this survey, and therefore below we report only comparisons among females (Table S4).

D. melanogaster females generally have smaller eyes (0.141±0.0134 mm^2) than those of the other species, being on average 15%, 17% and 24% smaller than *D. simulans* (0.166±0.0119 mm^2), *D. sechellia* (0.170±0.0178 mm^2) and *D. mauritiana* (0.185±0.0194 mm^2) eyes, respectively. However, *D. melanogaster* strains with the largest eyes have similar eye sizes to *D. simulans* and *D. sechellia*, particularly those from a Zambia (ZI) population (Fig. 1A; Tables S3, S4). This is unlikely to simply be explained by overall body size differences, however, because the surveyed *D. melanogaster* strains have on average larger tibias compared to the other species (Fig. S3A; Table S4).

In addition to differences in eye size between species, there is substantial intraspecific variation in this trait (Fig. 1, Table S4). Some of these differences may reflect

population based differences, as observed between the *D. melanogaster* strains from Rwanda (RG) compared to Zambia (ZI), with Rwanda female eyes (0.137±0.0096 mm^2) being on average 9% smaller than those of Zambia females (0.150±0.0121 mm^2) (Fig. 1, Table S4). Finally, differences in inter-ocular distance between species follow the opposite trend to eye area, consistent with the common negative correlation of these two traits in species of this subgroup (Fig. S3, Fig. S1, Table S4) (Norry *et al.* 2000; Posnien *et al.* 2012; Arif *et al.* 2013).

We then aimed to describe the genetic architecture underlying intraspecific eye size differences in both *D. melanogaster* and *D. simulans*. We focused on strains that differed significantly in eye area and that represented extremes of the surveyed variation: *D. melanogaster* ZI373 versus RG13N and *D. simulans* Tana10 versus *D. simulans* Zom4 (Table S3, Fig. S3A-B, D-E). Measured from frontal views of the head, *D. melanogaster* ZI373 females have eye area and inter-ocular distances on average 7% larger and 4% smaller, respectively, compared to RG13N (Table S3). *D. simulans* Tana10 females have eye area and inter-ocular distances on average 13% larger and 7% smaller, respectively, compared to Zom4 (Table S3). As expected, differences in eye size between the compared *D. melanogaster* and *D. simulans* strains are inverse to differences in inter-ocular distance (Fig. S3A-B, D-E).

We next investigated if these differences in eye size are caused by changes in ommatidia number and/or ommatidial diameter. In *D. melanogaster* females, the larger eyed strain ZI373 (779±49 ommatidia) has on average 121 more ommatidia than the RG13N strain (658±57 ommatidia). In *D. simulans* females, the larger eyes strain Tana10 (864±30 ommatidia) has on average 69 more ommatidia than the Zom4 strain (795±32 ommatidia) (Fig. 2A). The diameter of ommatidia varies across the eyes of individual flies (Fig. S5), and therefore to assess the contribution of differences in ommatidia size to overall eye size we measured the diameter of central ommatidia in each strain. Ommatidia

diameters are on average marginally wider in females of the strains of each species with smaller eyes, RG13N (18.95±0.522 µm) or Zom4 (19.04±0.589 µm), compared to ZI373 (17.70±0.718 µm) or Tana10 (18.65±0.476 µm), respectively (Fig. 2B). Therefore, larger eye size between the focal strains can be mostly attributed to differences in ommatidia number, rather than differences in ommatidia size.

Eye size differences between these strains could generally reflect differences in body size. In *D. melanogaster*, the larger eyed ZI373 strain has shorter tibias compared to the smaller eyed RG13N (Fig. S4C). In the analyzed *D. simulans* strains Zom4 and Tana10, tibia length differences are only significant for females but not males (Fig. S4F). We further estimated allometric coefficients (α) for the regression of eye area and inter-ocular distance with tibia length in these strains (Fig. S6). Eye area is either hyperallometric to tibia length in ZI373 and Zom4 or hypoallometric in RG13N and Tana10 (Fig. S6A, B). In contrast to eye area, inter-ocular distance is always hypoallometric to tibia length in all the analyzed strains ($\alpha<1$) (Fig. S6A', B'), suggesting different scaling relationships of these traits with body size. Overall, therefore, differences in eye size and inter-ocular distance between the focal strains of *D. melanogaster* and *D. simulans* are not simply just a reflection of body size.

To better describe shape differences between the head of the analyzed strains, we used PCA of the position of stereotypical landmarks on the heads (Fig. 2C). PC1 corresponded to differences in head posture during image acquisition and hence we discarded this PC (Posnien *et al.* 2012). We focused instead on the subsequent two main axes of variation, PC2 and PC3, each respectively explaining 19.54% and 5.3% of head shape variation between ZI373 and RG13N, and 28.03% and 6.69% of head shape variation between Tana10 and Zom4. Thin-plate splines interpolation indicates that significant differences in head shape occur in both sexes mostly along the medial-lateral axis between the *D. melanogaster* strains (Fig. 2C,D) and along the dorsal-ventral axis

between the *D. simulans* strains (Fig. 2C,E), suggesting different allocations of eye and head capsule fate along these axes between strains of the two species.

QTL mapping in D. melanogaster

To assess the fraction of eye size traits that can be attributed to genetic variation, we estimated narrow-sense heritability from a parent-offspring regression of eye size phenotypes, focusing on strains from a *D. melanogaster* ZI population. This revealed a weak correlation between progeny eye area or inter-ocular distance and the mid-parent phenotypes (eye area h^2=0.25, inter-ocular distance h^2=0.16, Fig. S7). This highlights a complex genetic architecture underlying eye size variation within this population, consistent with the polygenic basis of previously studied size-related quantitative traits.

In order to map QTL associated with eye and head size traits in *D. melanogaster,* we generated a mapping population of 192 F2 individuals generated from reciprocal crosses of the strains ZI373 and RG13N (see materials and methods). Interval mapping of eye area using Haley-Knott regression in *D. melanogaster*, taking tibia length and sex as covariates, identified one significant QTL on chromosome 3 at 3L:4.51 Mb (at genome-wide $P < 0.05$), explaining 3.9% of the phenotypic variance, with tibia length variation accounting for up to 29.5% of the phenotypic variance (Fig. 3A; Table 1). For inter-ocular distance, we found two significant QTL (at genome-wide $p < 0.05$), one on chromosome 2 at 2R:24.74 Mb and one on chromosome 3 at 3L:0.82 Mb, together explaining 9.3% of the phenotypic variance, with tibia length accounting for up to 30.2% of the phenotypic variance (Fig. 3B, Table 1). Given the proximity of the QTL on chromosome 3 at 3L:4.51 Mb for eye area and at 3L:0.82 Mb for inter-ocular distance, and the large 2-LOD confidence intervals for these QTL, we cannot exclude that these effects could be caused by the same locus (Table 1).

To further assess the effect of body size, we explored the association of tibia length

with eye size variation. Tibia length variation is mostly explained by QTL on chromosome 3, at 3L:0.82 Mb, 3R:15.3 Mb (T2 tibia) and 3L:6.01 Mb (T3 tibia), and one on chromosome 2, at 2L:9.01 Mb (T2 tibia). These QTL are in close proximity with prominent LOD peaks in the eye area and inter-ocular distance QTL maps (Fig. 3A-B, Fig. S8A-B, Table 1). With the exception of the QTL at 3L:0.82 Mb, in both the eye area and inter-ocular distance QTL maps these peaks are not significant at genome-wide level when considering tibia length as a covariate, indicating that they may represent the same loci underlying general body size variation (Fig. 3A-B). Furthermore, it is worth noting that all LOD scores for loci on the 2nd chromosome are higher in the mapping of eye area and inter-ocular distance when considering tibia length as a covariate, indicating a pervasive negative correlation between tibia length variation and eye size variation due to loci on this chromosome (Fig. 3A-B).

QTL mapping in D. simulans

We used a backcross design in *D. simulans* to generate a mapping population, where F1 female progeny of a cross between the strains Tana10 and Zom4 were crossed back to each of these parental strains (Fig. S2B). Interval mapping of eye area using Haley-Knott regression in the *D. simulans* Tana10 backcross, taking tibia length and sex as covariates, identified one significant QTL on chromosome 2 at 2R:4.98 Mb, and two on chromosome 3 at 3L:5.07 Mb and 3R:16.61 Mb (all at genome-wide $p < 0.05$) (Fig. 3C, Table 2). Tibia length variation can explain up to 80% of variation in eye area in this case, suggesting a large component of variation due to general body size variation. After accounting for this component, additive interactions between these QTL explain 5.5% of the phenotypic variance (Table 2). For inter-ocular distance, we identified two significant QTL in the Tana10 backcross, one on chromosome 2 at 2L:0.17 Mb, and one on chromosome 3 at 3R:20.07 Mb, together explaining 2.6% of the phenotypic variance after accounting for

tibia length variation, which explains up to 47.5% of variation in this case (Fig. 3D, Table 2).

Taking into account the 2-LOD confidence interval overlap, the QTL locations for eye area and inter-ocular distance variation are similar in the Zom4 backcross mapping population, with only an additional distinct QTL interval for inter-ocular distance at 3L:16.52 Mb (Fig. 3C-E,D-F, Table 2). This finding is consistent between QTL locations in both backcrosses, indicating co-dominance of these QTL. Additionally, 2-LOD confidence intervals were also largely overlapping for eye size and inter-ocular distance QTL on the right arm of chromosome 3 at 3R:16.61 Mb or 3R:15.04 Mb for eye area, and at 3R:20.07 Mb or 3R:19.72 Mb, for inter-ocular distance, suggesting that they may represent the same locus. Thus, with regards to these QTL, there may be common genetic bases for eye area and inter-ocular distance variation. (Fig. 3C-F, Table 2).

In both backcrosses, several QTL for tibia length were also detected above genome-wide significance ($p < 0.05$) on the X chromosome, and an additional QTL underlying variation in the length of T2 tibia was detected at 2R:15.55 Mb (Fig. S8C-F, Table 2). 2-LOD confidence intervals suggest overlap between the X chromosome QTL, suggesting that they may represent a single locus. However, these are not detected above genome-wide significance in the eye area and inter-ocular distance QTL maps, perhaps reflecting independent genetic mechanisms that regulate general body size and eye or head size (Table 2).

Interestingly, the 2-LOD confidence interval of the QTL underlying variation of the T2 tibia length at 2R:15.55 Mb overlaps with the QTL underlying eye area variation identified on chromosome 2 in both backcrosses. This may be a common feature with QTL on chromosome 2 in the *D. melanogaster* QTL map (Fig. 3A,C,E, Fig. S8A,C, Tables 1-2). Both the *D. melanogaster* and *D. simulans* QTL maps also show similar eye area QTL locations on the left end of chromosome 3, at 3L:4.51 Mb in *D. melanogaster* and at

3L:5.07 Mb or 3L:6.09 Mb in *D. simulans*, suggesting possible similarities in the genetic architecture of eye size variation across species (Tables 1 and 2).

The development of eye size differences

Differences in eye size may arise as a consequence of changes in the trade-off between different parts of the head capsule during growth and differentiation of the eye-antenna disc. In order to better understand the developmental basis of eye size differences between the selected strains of *D. melanogaster* and *D. simulans* used for mapping, we analyzed eye-antennal discs at 96 hours after egg laying (AEL), when the morphogenetic furrow has moved about halfway across the presumptive retinal field. We measured the relative sizes of the eye progenitor field, as marked by expression of the retinal determinant Eya, and the differentiated part of the eye, as marked by the neuronal marker Elav (Fig. 4). In *D. melanogaster* there is a clear difference in the relative size of the eye progenitor field between the ZI373 and RG13N strains, with the size of the Eya-positive domain being bigger in the larger eyes strain ZI373 (Fig. 4A, E-H). Additionally, the strain RG13N shows a bigger Elav-positive domain both relative to the size of the whole disc in females and to the size of the Eya-positive domain in both sexes, suggesting faster differentiation of the retina in this strain compared to ZI373 (Fig. 4A-B, E-H). These observations suggest that eye size differences between ZI373 and RG13N may arise from differences in the number of cells committed to become eye progenitors and differences in the speed of retinal differentiation. However, at 96 hours AEL in *D. simulans,* we found no significant difference in the relative size of the Eya-positive domain between the Zom4 and Tana10 strains, suggesting that, in this case, differences in eye size arise later in development (Fig. 4C, I-L). The size of the entire eye-antenna disc is only slightly larger in males of the Tana10 strain relative to the Zom4 strain and this is also reflected in the size of the Elav-positive domain relative to the whole disc or the eye progenitor field (Fig. 4C-

D). These results suggest differences in the temporal dynamics of eye fate determination between the analyzed *D. melanogaster* and *D. simulans* strains, with those differences being detected already at 96h AEL in *D. melanogaster* but not in *D. simulans.* These differences in development are suggestive of underlying differences in the genetic bases of variation in adult eye size between *D. melanogaster* and *D. simulans.*

Discussion

Natural variation in fly eye and head morphology

We have extended previous surveys of eye size variation within and between species of the *D. melanogaster* subgroup (Norry *et al.* 2000; Hämmerle and Ferrús 2003; Posnien *et al.* 2012; Arif *et al.* 2013; Hilbrant *et al.* 2014; Ramaekers *et al.* 2018). Our findings emphasise the extensive natural variation in eye size that can be caused by differences in ommatidia number and ommatidia diameter. We further substantiate that *D. melanogaster* eyes tend to be smaller than its sibling species and confirm the previous finding that *D. mauritiana* tends to have largest eyes in the *melanogaster* subgroup (Sturtevant 1919; Manning 1960; Watada M, Ohba S, Tobari 1986; McNamee and Dytham 1993; Posnien *et al.* 2012; Arif *et al.* 2013; Hilbrant *et al.* 2014).

We also found that there is considerable variation in ommatidia number between strains of *D. melanogaster* and *D. simulans*, with differences of up to 121 ommatidia (Fig. 2A). These differences may contribute to variation in visual acuity as it has been shown that higher numbers of ommatidia tend to increase acuity (Currea *et al.* 2018; Ramaekers *et al.* 2018). In addition, this may result in eyes with proportionally more of the 'pale' ommatidial subtype that detects short wavelengths in the UV and blue light ranges (Hilbrant *et al.* 2014). Interestingly, decreasing eye size in *D. melanogaster* via nutritional restriction can result in differences of up to 430 ommatidia with little change in spatial acuity or contrast sensitivity because of compensation by neural summation at the

expense of temporal acuity (Currea *et al.* 2018). We also found that flies with relatively more ommatidia have narrower ommatidia and vice versa, for example in the case of *D. melanogaster* strain RG13N compared to ZI373. This suggests that ommatidia diameter and number may be influenced by how they are packed and organized in the developing eye. These changes in ommatidial diameter are also expected to have an impact on the distribution of inter-ommatidial angles across the eye, and thus contribute to differences in vision. Indeed, differences in inter-ommatidial angles from the center to the periphery of the eye have been described to have an important impact on spatial acuity in other dipterans, including houseflies, hoverflies and blow-flies (Land 2009). For instance, predator flies of the genus *Coenosia* display high spatial acuity and sharp gradients of inter-ommatidial angles from the center to the periphery of the eye, compared to their *Drosophila* prey (Gonzalez-Bellido *et al.* 2011). Therefore in future, it will be interesting to explore if the differences in ommatidia number and diameter that we have found also result in changes to spatial acuity and contrast sensitivity, or if these are also buffered by neural summation, as during nutritional restriction.

Finally, consistent with previous studies, we have found that there is a negative correlation between eye size and other head capsule traits like face width or inter-ocular distance (Norry *et al.* 2000; Hämmerle and Ferrús 2003; Posnien *et al.* 2012; Arif *et al.* 2013). Therefore, there generally appears to be a developmental trade-off between eye and head capsule size, potentially to constrain overall head size perhaps to preserve aerodynamics. It has previously been shown that different loci of large effect contribute to eye size and inter-ocular distance variation (Arif *et al.* 2013) and this may explain why these two traits can evolve independently in some lineages of flies (Grimaldi and Fenster 1989; Wilkinson and Reillo 1994; Sukontason *et al.* 2008).

The genetic basis of eye size may differ within and between Drosophila species

To further explore the genetic basis of eye size differences and the trade-off with other head capsule traits, we mapped intra-specific variation in eye size between strains of *D. melanogaster* and *D. simulans* that differ mainly in ommatidia number (Fig. 3, Tables 1-2). In agreement with previous studies of eye size variation in *D. melanogaster* (Vonesch *et al.* 2016; Norry and Gomez 2017), we found that the eye differences between African strains of *D. melanogaster* and *D. simulans* are polygenic, supported by a low population level narrow sense heritability and low variance of head traits explained by fewer than 3 or 4 genome-wide significant QTL (Fig. S7, Tables 1-2). Interestingly, 2-LOD support intervals of QTL above genome-wide significance seem to roughly overlap across species, for example in the case of QTL at the left end of chromosome 3. This suggests the possibility that common genetic factors underlie within and between-species differences in the cases analyzed. However, we have found evidence that different developmental mechanisms underlie natural variation in eye size within *D. melanogaster* and *D. simulans* (Fig. 4), which implies that different genes or different variation within the same gene underlie differences between species.

The same loci may underlie reciprocal changes in eye size and inter-ocular distance

Our mapping results in both *D. melanogaster* and *D. simulans* have revealed similar estimates for the locations of QTL underlying eye area and inter-ocular distance variation, thus suggesting the same genes underlie the apparent trade-off between these traits. This contrasts with the previous observation of independent large-effect QTL underlying variation between *D. simulans* and *D. mauritiana* eye size and inter-ocular distance variation (Arif *et al.* 2013). However, this could be explained by differences in eye size being caused by changes in ommatidia diameter on one hand versus ommatidia number on the other, where in the latter case the same gene(s) could increase the number of retinal cells and directly decrease the number of face cuticle cells. To address this in the

future will require higher resolution mapping to identify the causative genes and test if they contribute to differences in both traits.

Evolution of the gene regulatory network for eye size

It was previously shown that a SNP (*Dmel*r6.25 4:710326) in the regulatory region of *ey*, which is on the 4th chromosome, explains variation in eye size as a result of ommatidia number differences between *D. melanogaster* strains CantonS and HickonAS, and also the larger eyes of *D. pseudoobscura*, with the A-allele variant being associated with larger eyes and the G-variant with smaller eyes (Ramaekers *et al.* 2018). The *D. melanogaster* strains ZI373 and RG13N analyzed in this study both have the G-allele variant, and the *D. simulans* strains Tana10 and Zom4 both have the A-allele variant, thus indicating that variation in this allele doesn't contribute to differences between these strains. However, we cannot exclude that differences in the allele variant at this SNP between *D. melanogaster* and *D. simulans* may contribute to differences in eye size observed between these species, since *D. simulans* generally have larger eyes and the strains used for mapping carry the large eye A-allele.

In addition, given previous studies and our findings that eye size differences are polygenic in *D. melanogaster and D. simulans,* with QTL on the 2nd and 3rd chromosomes, this suggests that the gene regulatory network that specifies eye size can evolve at multiple different nodes. Therefore, it will now be very interesting to build on our study to identify the genes that underlie these differences in eye size in different lineages, where they are located in the gene regulatory network, and how variation at these loci contribute to the developmental changes that produce different numbers of ommatidia and variation in eye size. This will provide further insights into the evolution of the gene regulatory networks underlying phenotypic changes more generally, particularly those for organ shape and size (Stern and Orgogozo 2008, 2009; Stern 2010; Courtier-Orgogozo and

Martin 2017; Kittelmann *et al.* 2018).

Acknowledgements

This work was funded by ERC (242553) and BBSRC (BB/M020967/1) grants to A.P.M. We thank the lab of John Pool for kindly providing *D. melanogaster* strains from Zambia (ZI) and Rwanda (RG) populations and we thank the lab of Christian Schlötterer for kindly providing *D. simulans* and *D. mauritiana* strains. We thank Linta Kuncheria for help with phenotyping of the *D. simulans* QTL mapping population and Madeleine Lindsay for help with face landmark registration. Synchrotron radiation beam time was provided by the Paul Scherrer Institut, Villigen, Switzerland, at beamline TOMCAT of the SLS and we would like to thank Christian Schlepütz for his assistance.

Literature cited

Adams D. C., and E. Otárola-Castillo, 2013 Geomorph: An r package for the collection and analysis of geometric morphometric shape data. Methods Ecol. Evol. 4: 393–399. https://doi.org/10.1111/2041-210X.12035

Andolfatto P., D. Davison, D. Erezyilmaz, T. T. Hu, J. Mast, *et al.*, 2011 Multiplexed shotgun genotyping for rapid and efficient genetic mapping. Genome Res. 21: 610–617. https://doi.org/10.1101/gr.115402.110

Arif S., M. Hilbrant, C. Hopfen, I. Almudi, M. D. S. Nunes, *et al.*, 2013 Genetic and developmental analysis of differences in eye and face morphology between Drosophila simulans and Drosophila mauritiana. Evol. Dev. 15: 257–267. https://doi.org/10.1111/ede.12027

Broman K. W., H. Wu, Ś. Sen, and G. A. Churchill, 2003 R/qtl: QTL mapping in experimental crosses. Bioinformatics 19: 889–890. https://doi.org/10.1093/bioinformatics/btg112

Burkhardt D., and I. de la Motte, 1988 Big “antlers” are favoured: female choice in stalk-eyed flies (Diptera, Insecta), field collected harems and laboratory experiments. J. Comp. Physiol. A 162: 649–652. https://doi.org/10.1007/BF01342640

Cotton S., J. Small, R. Hashim, and A. Pomiankowski, 2010 Eyespan reflects reproductive quality in wild stalk-eyed flies. Evol. Ecol. 24: 83–95. https://doi.org/10.1007/s10682-009-9292-6

Cotton A. J., M. Földvári, S. Cotton, and A. Pomiankowski, 2014 Male eyespan size is associated with meiotic drive in wild stalk-eyed flies (Teleopsis dalmanni). Heredity (Edinb). 112: 363–369. https://doi.org/10.1038/hdy.2013.131

Courtier-Orgogozo V., and A. Martin, 2017 Predicting the genetic loci of past evolution. bioRxiv, https://doi.org/10.1101/205153

Crick F. H. C., and P. A. Lawrence, 1975 Compartments and polyclones in insect development. Science 189: 340–347. https://doi.org/10.1126/science.806966

Currea J. P., J. L. Smith, and J. C. Theobald, 2018 Small fruit flies sacrifice temporal acuity to maintain contrast sensitivity. Vision Res. 149: 1–8. https://doi.org/10.1016/j.visres.2018.05.007

Domínguez M., and F. Casares, 2005 Organ specification-growth control connection: New in-sights from the Drosophila eye-antennal disc. Dev. Dyn. 232: 673–684. https://doi.org/10.1002/dvdy.20311

Garcia-Bellido A., P. Ripoll, and G. Morata, 1973 Developmental compartmentalisation of the wing disk of drosophila. Nat. New Biol. 245: 251–253. https://doi.org/10.1038/newbio245251a0

Gonzalez-Bellido P. T., T. J. Wardill, and M. Juusola, 2011 Compound eyes and retinal information processing in miniature dipteran species match their specific ecological demands. Proc. Natl. Acad. Sci. 108: 4224–4229. https://doi.org/10.1073/pnas.1014438108

Grimaldi D., and G. Fenster, 1989 Evolution of extreme sexual dimorphisms: Structural and behavioural convergence among broad-headed male Drosophilidae (Diptera). Am. Museum Novit. http://hdl.handle.net/2246/5094

Haley C. S., and S. A. Knott, 1992 A simple regression method for mapping quantitative trait loci in line crosses using flanking markers. Heredity (Edinb). 69: 315–324. https://doi.org/10.1038/hdy.1992.131

Hämmerle B., and A. Ferrús, 2003 Expression of enhancers is altered in Drosophila melanogaster hybrids. Evol. Dev. 5: 221–230. https://doi.org/10.1046/j.1525-142X.2003.03030.x

Hilbrant M., I. Almudi, D. J. Leite, L. Kuncheria, N. Posnien, *et al.*, 2014 Sexual dimorphism and natural variation within and among species in the Drosophila retinal mosaic. BMC Evol. Biol. 14. https://doi.org/10.1186/s12862-014-0240-x

Hingle A., K. Fowler, and A. Pomiankowski, 2001 Size-dependent mate preference in the stalk-eyed fly Cyrtodiopsis dalmanni. Anim. Behav. 61: 589–595. https://doi.org/10.1006/anbe.2000.1613

Kaneshiro K. Y., and C. R. B. Boake, 1987 Sexual selection and speciation: Issues raised by Hawaiian Drosophila. Trends Ecol. Evol. 2: 207–212. https://doi.org/10.1016/0169-5347(87)90022-X

Kittelmann S., A. D. Buffry, F. A. Franke, I. Almudi, M. Yoth, *et al.*, 2018 Gene regulatory network architecture in different developmental contexts influences the genetic basis of morphological evolution. PLoS Genet. 14. https://doi.org/10.1371/journal.pgen.1007375

Land M. F., 2002 VISUAL ACUITY IN INSECTS. Annu. Rev. Entomol. 42: 147–177. https://doi.org/10.1146/annurev.ento.42.1.147

Land M. F., 2009 Eyes and Vision, pp. 345–355 in *Encyclopedia of Insects*. Academic Press

Land, M.F.; Nilsson D. E., 2012 *Animal eyes*. Oxford University Press.

Manning A., 1960 The Sexual Behaviour of Two Sibling Drosophila Species. Behaviour 15: 123–145. https://doi.org/10.1163/156853960X00133

McNamee S., and C. Dytham, 1993 Morphometric discrimination of the sibling species Drosophila melanogaster (Meigen) and D. simulans (Sturtevant) (Diptera: Drosophilidae). Syst. Entomol. 18: 231–236. https://doi.org/10.1111/j.1365-3113.1993.tb00663.x

Norry F. M., J. C. Vilardi, and E. Hasson, 2000 Negative genetic correlation between traits of the Drosophila head, and interspecific divergence in head shape. Heredity (Edinb). 85: 177–183. https://doi.org/10.1046/j.1365-2540.2000.00735.x

Norry F. M., and F. H. Gomez, 2017 Quantitative trait loci and antagonistic associations for two developmentally related traits in the drosophila head. J. Insect Sci. 17. https://doi.org/10.1093/jisesa/iew115

Pool J. E., R. B. Corbett-Detig, R. P. Sugino, K. A. Stevens, C. M. Cardeno, *et al.*, 2012 Population Genomics of Sub-Saharan Drosophila melanogaster: African Diversity and Non-African Admixture. PLoS Genet. 8. https://doi.org/10.1371/journal.pgen.1003080

Posnien N., C. Hopfen, M. Hilbrant, M. Ramos-Womack, S. Murat, *et al.*, 2012 Evolution of eye morphology and Rhodopsin expression in the Drosophila melanogaster species subgroup. PLoS One 7. https://doi.org/10.1371/journal.pone.0037346

Ramaekers A., S. Weinberger, A. Claeys, M. Kapun, and J. Yan, 2018 Altering the temporal regulation of one transcription factor drives sensory trade-offs. bioRxiv, https://doi.org/10.1101/348375.

Riska B., 1986 Some models for development, growth and morphometric correlation. Evolution 40: 1303–1311. https://doi.org/10.1111/j.1558-5646.1986.tb05753.x

Spieth H. T., 1981 Drosophila heteroneura and Drosophila sylvestris: Head shapes, behaviour and evolution. Evolution. 35: 921–930. https://doi.org/10.1111/j.1558-

5646.1981.tb04958.x

Stern D. L., and V. Orgogozo, 2008 The loci of evolution: How predictable is genetic evolution? Evolution. 62: 2155–2177. https://doi.org/10.1111/j.1558-5646.2008.00450.x

Stern D. L., and V. Orgogozo, 2009 Is genetic evolution predictable? Science. 323: 746–751. https://doi.org/10.1126/science.1158997

Stern D. L., 2010 *Evolution, Development and the Predictable Genome*. Roberts and Company Publishers.

Sturtevant A. H., 1919 A New Species Closely Resembling Drosophila Melanogaster. Psyche (New York) 26: 153–155. https://doi.org/10.1155/1919/97402

Sukontason K. L., T. Chaiwong, S. Piangjai, S. Upakut, K. Moophayak, *et al.*, 2008 Ommatidia of blow fly, house fly, and flesh fly: Implication of their vision efficiency. Parasitol. Res. 103: 123–131. https://doi.org/10.1007/s00436-008-0939-y

Templeton A. R., 1977 Analysis of head shape differences between two interfertile species of hawaiian Drosophila. Evolution 31: 630–641. https://doi.org/10.1111/j.1558-5646.1977.tb01052.x

Theobald J. C., E. J. Warrant, and D. C. O'Carroll, 2010 Wide-field motion tuning in nocturnal hawkmoths. Proc. R. Soc. B Biol. Sci. 277: 853–860. https://doi.org/10.1098/rspb.2009.1677

Val, 1977 Genetic analysis of morphological differences between two interfertile species of hawaiian Drosophila. Evolution 31: 611–629. https://doi.org/10.1111/j.1558-5646.1977.tb01051.x

Vonesch S. C., D. Lamparter, T. F. C. Mackay, S. Bergmann, and E. Hafen, 2016 Genome-Wide Analysis Reveals Novel Regulators of Growth in Drosophila melanogaster. PLoS Genet. 12. https://doi.org/10.1371/journal.pgen.1005616

Watada M, Ohba S, Tobari Y. ., 1986 Genetic differentiation in Japanese populations of

Drosophila simulans and D. melanogaster. II. Morphological variation. Jpn J Genet 61: 469–480. https://doi.org/10.1266/jjg.61.469

Wilkinson G. S., and P. R. Reillo, 1994 Female choice response to artificial selection on an exaggerated male trait in a stalk-eyed fly. Proc. R. Soc. B Biol. Sci. 255: 1–6. https://doi.org/10.1098/rspb.1994.0001

Figures

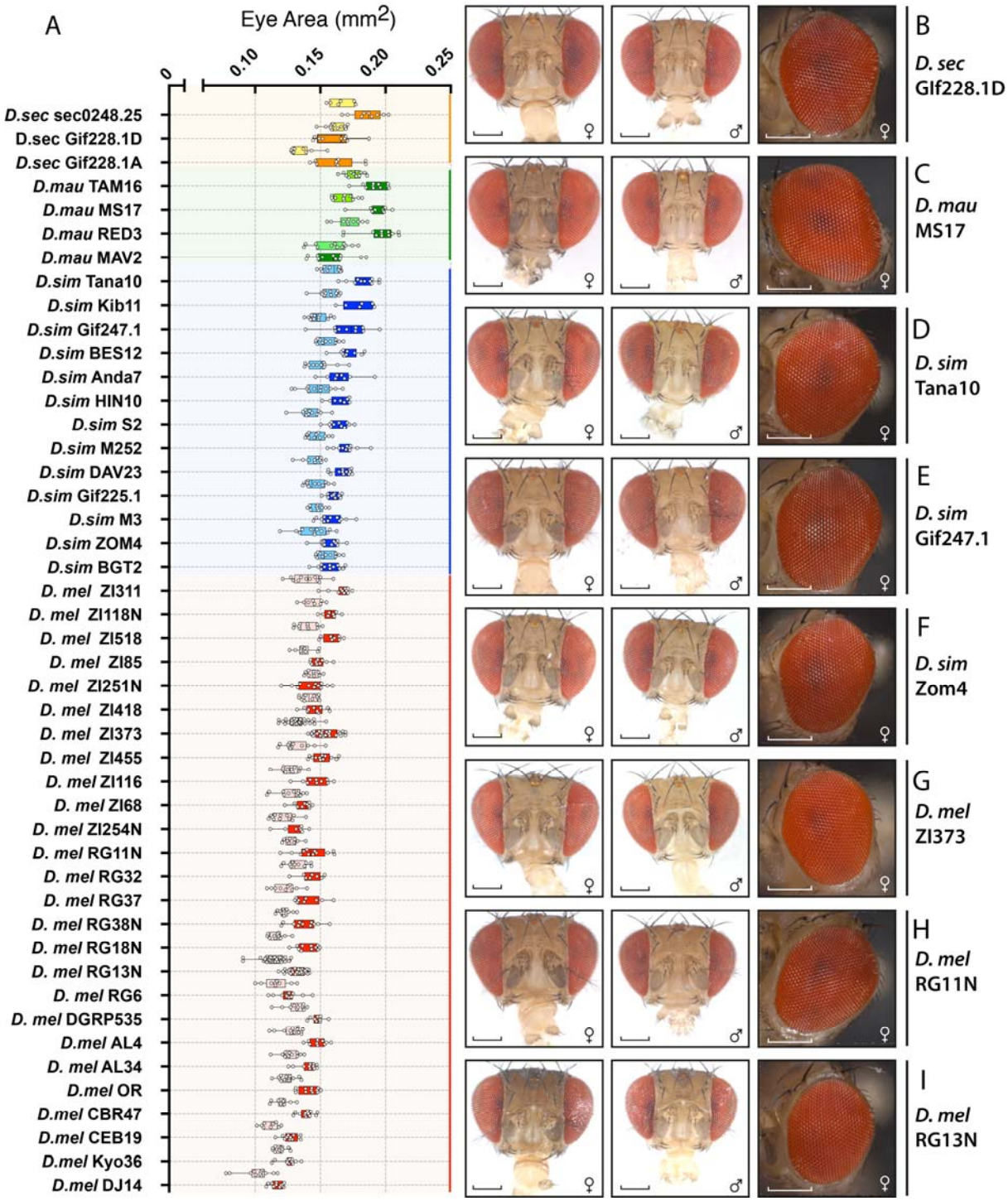

Fig. 1 – **Survey of eye size variation in the *D. melanogaster* species subgroup.**

(A) Box and whisker diagram of eye area (mm^2) distribution in strains of *D. melanogaster* (females – red, males - pink), *D. simulans* (females – dark blue, males – light blue), *D.*

mauritiana (females – dark green, males – light green) and *D. sechellia* (females – orange, males - yellow). (B-I) Frontal and lateral head views of females (♀) or males (♂) from strains representative of the average of the surveyed eye size variation in *D. sechellia* (B – *D. sec* Gif.228.1D) and *D. mauritiana* (C – *D. mau* MS17) and at the extremes and average of the surveyed variation in *D. simulans* (D – *D. sim* Tana10; E – *D. sim* Gif247.1; F – *D. sim* Zom4) and *D. melanogaster* (G – *D. mel* ZI373; H – *D. mel* RG11N; I – *D. mel* RG13N). scale bar – 200µm (see Table S3 for sample sizes).

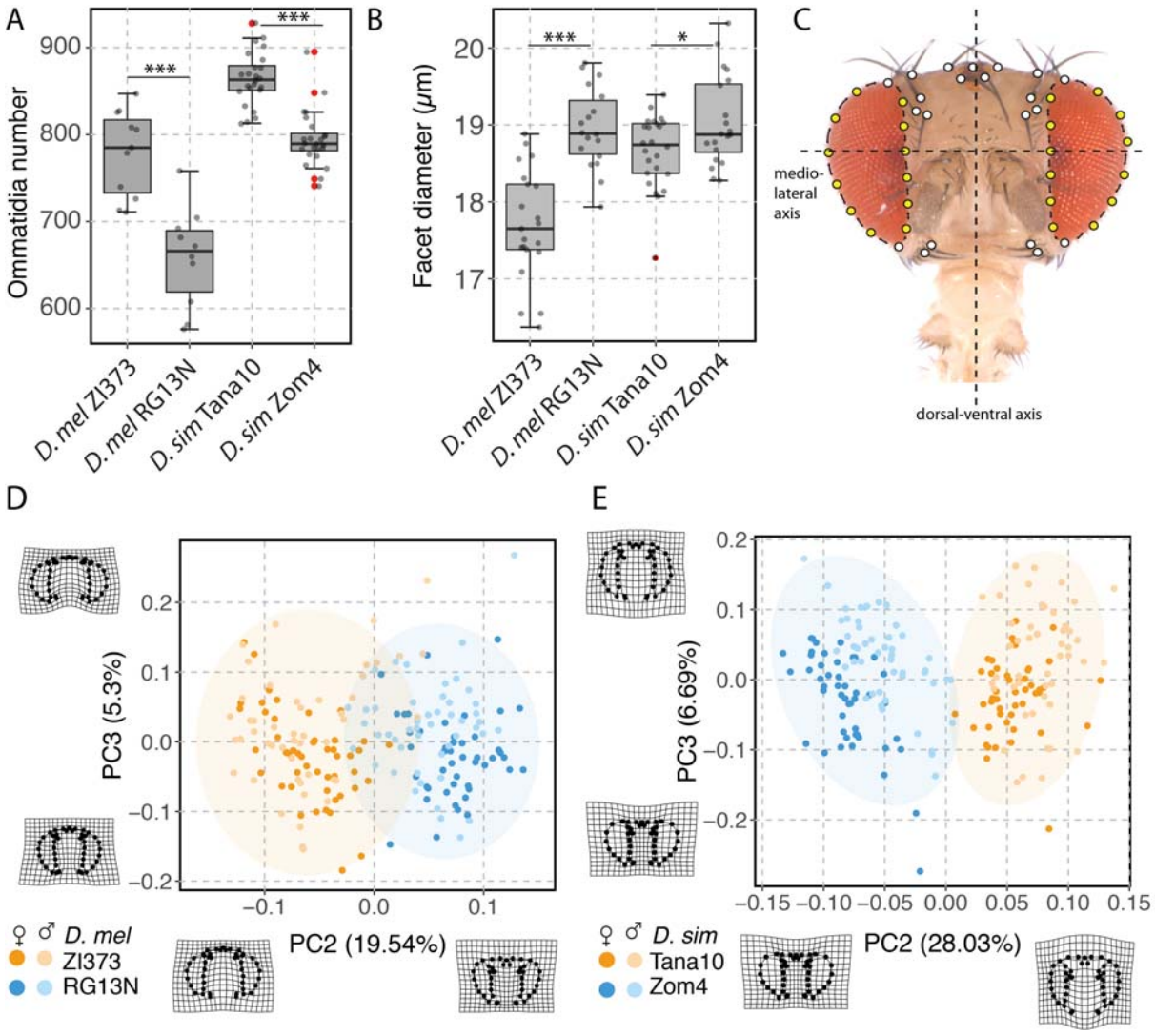

Fig. 2 – **Characterization of the ommatidial bases of eye size and shape differences in the focal strains.**

(A) Ommatidia number distribution in females of the strains ZI373 (n=11), RG13N (n=10), Tana10 (n=23) and Zom4 (n=24). (B) Average ommatidia diameter (μm) from central ommatidia (n=10) across strains ZI373 (n=21), RG13N (n=18), Tana10 (n=24) and Zom4 (n=20). (C) Position of landmarks (white) and semi-landmarks (yellow) along the front view of a *Drosophila* head used for PCA of head shape. (D) Distribution of PC2 and PC3 and their 95% confidence ellipses for position of head landmarks of the *D. melanogaster* strains ZI373 (orange) and RG13N (blue). (D) Distribution of PC2 and PC3 and their 95% confidence ellipses for position of head landmarks of the *D. simulans* strains Tana10

(orange) and Zom4 (blue). In (A-B), red data points represent outliers. In (D-E) lighter coloured lines and data points represent male data. Statistical comparisons represent t-tests: *** $p<0.0001$; *$p<0.01$.

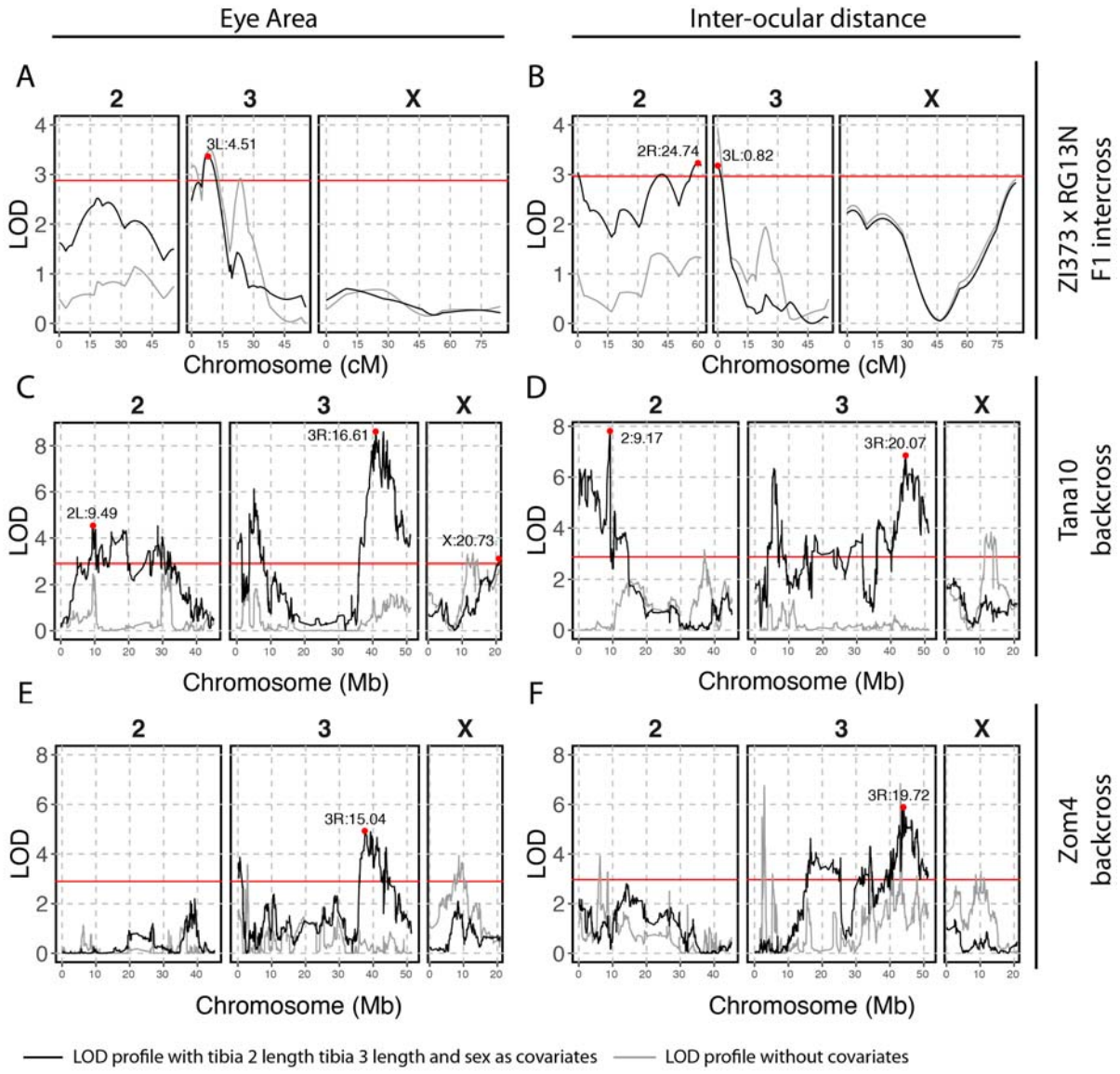

Fig.3 – QTL maps for eye area and inter-ocular distance.

(A) Eye area and (B) inter-ocular distance QTL maps for *D. melanogaster* F2 progeny from reciprocal crosses between strains ZI373 and RG13N (n=192). (C) Eye area and (D) inter-ocular distance QTL maps of a *D. simulans* backcross to the strain Tana10 (n=192). (C) Eye area and (D) inter-ocular distance QTL maps of *D. simulans* progeny from backcross to the strain Zom4 (n=192). A grey line represents LOD profiles without covariates and a black line indicates LOD profiles with sex and the T2 and T3 tibia lengths as covariates. A red horizontal line in each plot represents the genome-wide significance LOD threshold of p=0.05. The highest QTL peak above genome-wide significance (p<0.05) for each

chromosome is highlighted as a red dot and their location estimate is indicated above in Mb, according to *Dmel*r.6.45 for *D. melanogaster* and *Dsim*r2.01 for *D. simulans*. Note that the 4th chromosome is not shown but no significant QTL were detected on this chromosome in any of our mapping experiments.

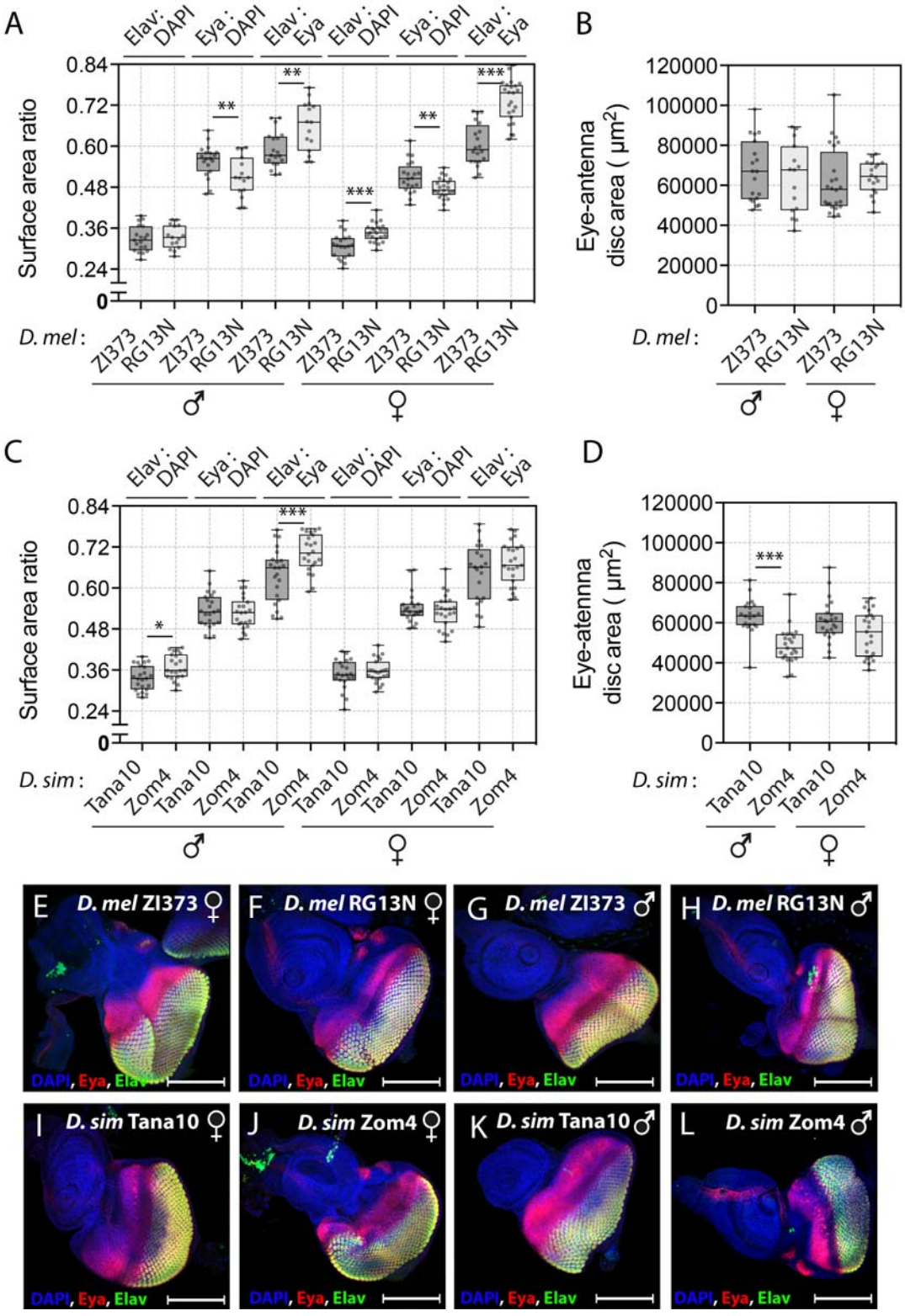

Fig.4 – Eye fate specification at 96h AEL in *D. melanogaster* and *D. simulans*.

(A,C) Surface area ratios between the Elav, Eyes absent (Eya) and DAPI labeled regions of the eye antenna disc and (B, D) whole disc areas (µm^2) in males (♂) and females (♀) of

the *D. melanogaster* strains ZI373 and RG13N and (A-B) and the *D. simulans* strains Tana10 and Zom4, at 96h AEL. (E-F') Eye-antennal discs, dissected at 96h AEL, of males (♂) and females (♀) of the *D. melanogaster* strains ZI373 (E-F), RG13N (F-H) and *D. simulans* strains Tana10 (I-J) and Zom4 (K-L), stained with Elav (green), Eya (red) and DAPI (blue). Scale bar = 200 µm. Statistical comparisons represent t-tests: ***p<0.0001, **p<0.001, *p<0.01.

Table 1. *D. melanogaster* QTL for eye area, inter-ocular distance and tibia length

Trait	QTL (Chr:Mb)	Peak Significance (LOD)	2LOD Support Region[1]			QTL Effects		
			Range (Mb)	Start (bp)	End (bb)	Standardized Additive Effect[2]	Standardized Dominant Effect[3]	Variance Explained (%)
Eye area	3L:4.51	2.487	8.35	3L: 4512922	3R: 18043455	0.20	0.06	3.931
Inter-ocular distance	2R:24.74	4.251	47.60	2L: 661886	2R: 24746955	0.31	-0.11	6.322
	3L:0.82	3.939	2.080	3L: 821255	3L: 10527569	0.11	0.13	3.011
Tibia 2 length	2L:9.01	5.553	10.35	2L: 661886	2L: 21292443	-0.37	0.10	5.905
	3L:0.82	1.452	41.53	3L: 821255	3R: 153094825	0.04	0.13	1.467
	3R:15.30	2.628	22.58	3L: 6019468	3R: 29777199	-0.13	0.25	2.694
Tibia 3 length	2L:1.63	2.203		2L: 661886	2R: 24746955	-0.23	0.02	2.638
	3L:6.01	5.051	50.34	3L: 821255	3R: 21255695	-0.12	0.36	6.268

[1]Regions corresponding to the 2-LOD support interval based on the next marker position closest to the interval boundaries.

[2, 3]See Materials and Methods for details on how these different measures of effect size were calculated.

Table 2. *D. simulans* QTL for eye area, inter-ocular distance and tibia length

Backcross to	Trait	QTL (Chr:Mb)	Peak Significance (LOD)	2LOD Support Region[1]			QTL Effects	
				Range (Mb)	Start (Chr:bp)	End (Chr:bp)	Standardized Additive Effect[3]	Variance Explained (%)
Tana10	Eye area	2R:4.98	6.827	18.97	2L: 14565193	2R: 10003506	-0.29	1.859
		3L: 5.07	7.463	6.62	3L: 222390	3L: 6848278	-0.30	2.040
		3R:16.61	5.934	4.23	3R: 15762354	3R: 19993526	-0.27	1.606
	Inter-ocular distance	2L:9.17	1.604	0.69	2L: 8534775	2L: 9230800	0.14	1.109
		3R:20.07	2.160	15.33	3R: 11539997	3R: 26876957	0.16	1.499
	Tibia 2 length	2R:13.34	3.383	26.98	2L: 11097565	2R: 14544480	0.20	4.105
		X@13.14	4.222	3.86	X: 10983391	X: 14850706	*	5.151
	Tibia 3 length	X@14.03	3.169	4.14	X: 10983391	X: 15127792	*	4.050
Zom4	Eye area	2R:15.55	1.197	13.61	2R: 3142925	2R: 16758197	0.12	0.298
		3L:6.09	2.567	1.34	3L: 158421	3L: 1508312	0.18	0.645
		3R:15.04	4.187	7.82	3R: 11909323	3R: 19729904	0.23	1.063
	Inter-ocular distance	2L:14.02	1.620	40.93	2L: 173606	2R: 6089451	-0.14	0.650
		3L:16.52	2.302	19.00	3L: 15245955	3R: 10095730	-0.17	0.928

	3R:19.72	2.580	7.46	3R: 17834324	3R: 25297963	-0.18	1.042
Tibia 2 length	X@10.95	4.508	3.31	X: 8109102	X: 11423981	*	5.371
Tibia 3 length	X@8.63	4.057	10.25	X: 4749425	X: 15000162	*	4.847

[1]Regions corresponding to the 2-LOD support interval based on the next marker position closest to the interval boundaries and base pair (bp) coordinates are given based on the *D. simulans* genome r2.0.2.

[2]Number of genes in the 2-LOD support interval based on the r2.0.2_FB2017_04 annotation of *D. simulans* genome.

[3]See Materials and Methods for details on how these different measures of effect size were calculated.

* X-chromosome QTL effect sizes are not interpreted in this table because these are subdivided into individual effects in female homozygotes, female heterozygotes and males.

Supplementary Figures

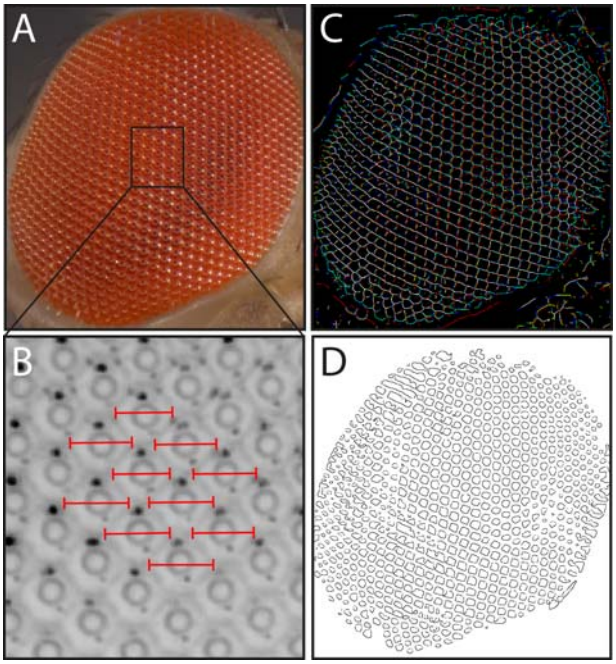

Fig. S1 – Measurement of ommatidia size and number.

(A) Extended depth of focus projection of a lateral view of the *Drosophila* head (ZI373 female). (B) Close-up view of central facets, showing in red the diameter measurement taken for a cluster of 10 ommatidia. (C) Valleys segmentation of a lateral head view (A), used for (D) particle counting of ommatidia number.

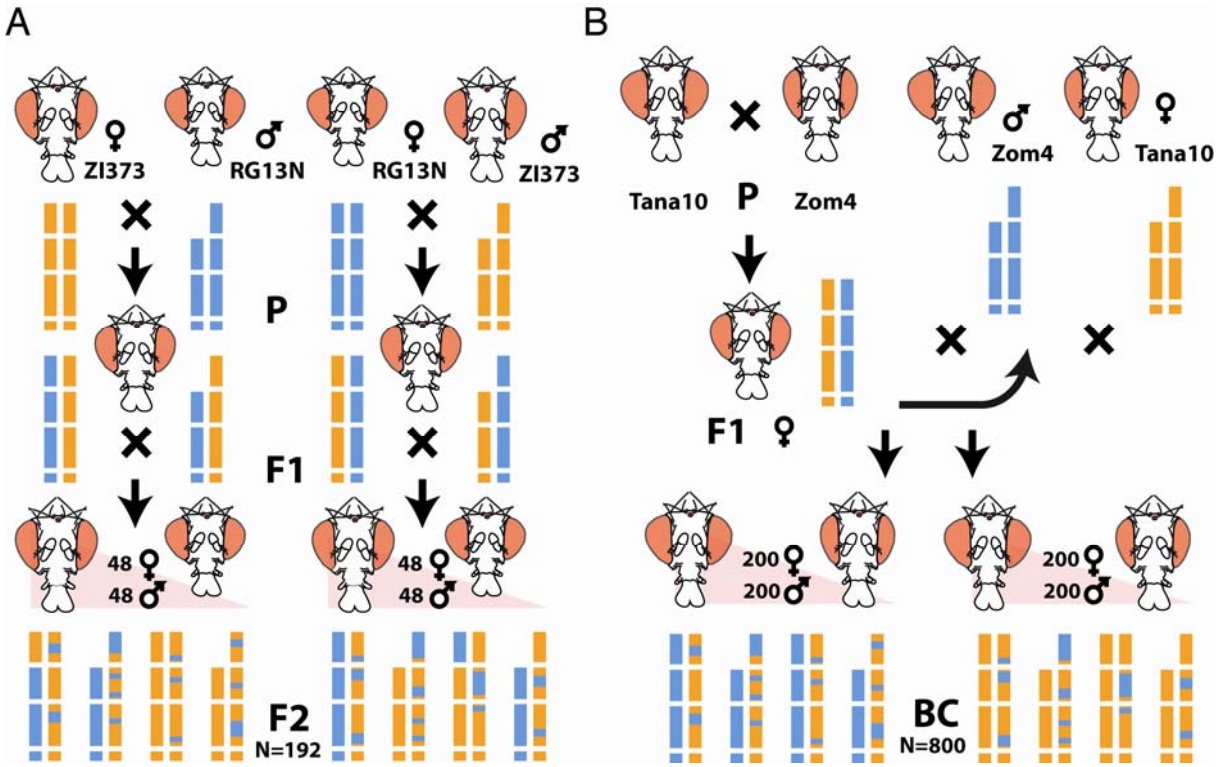

Fig. S2 – QTL mapping cross designs.

(A) F2 design for crosses between the *D. melanogaster* strains ZI373 (orange) and RG13N (blue), representing the generation of 192 F2 individuals, 48 of which were male and 48 female. (B) Backcross design for crosses between the *D. simulans* strains Tana10 (orange) and Zom4 (blue), representing the generation of backcross (BC) individuals, 384 from each backcross direction, each with 192 females and 192 males. Separate vertical bars coloured according to expected genotypes represent the three autosomes and the X chromosome.

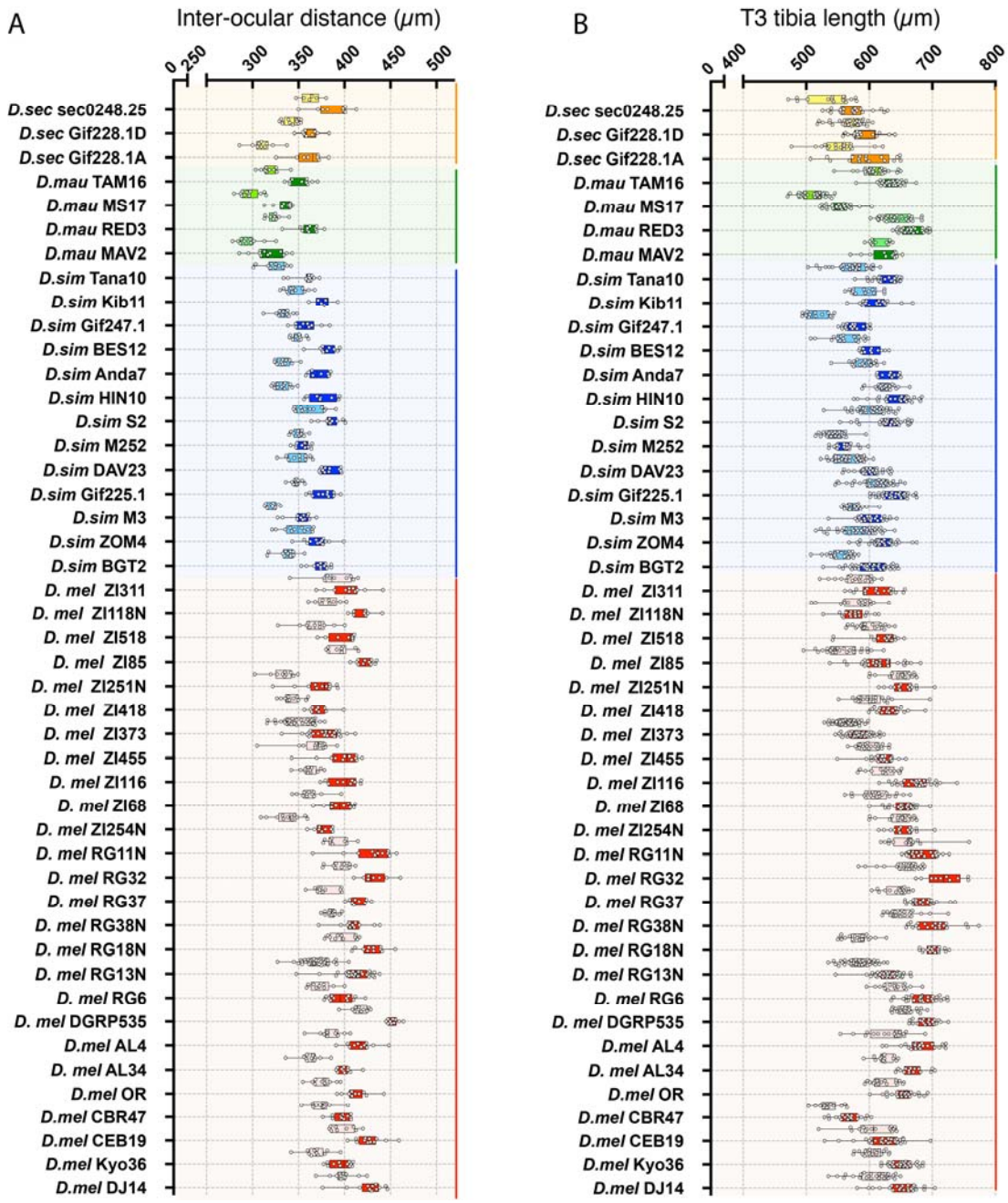

Fig. S3 – **Survey of inter-ocular distance and T3 tibia length in the *D. melanogaster* species subgroup.**

(A) Box and whisker diagram of inter-ocular distance (μm) (B) and posterior tibia length (μm) distribution in strains of *D. melanogaster* (females – red, males - pink), *D. simulans* (females – dark blue, males – light blue), *D. mauritiana* (females – dark green, males – light green) and *D. sechellia* (females – orange, males - yellow) (see Table S3 for sample sizes).

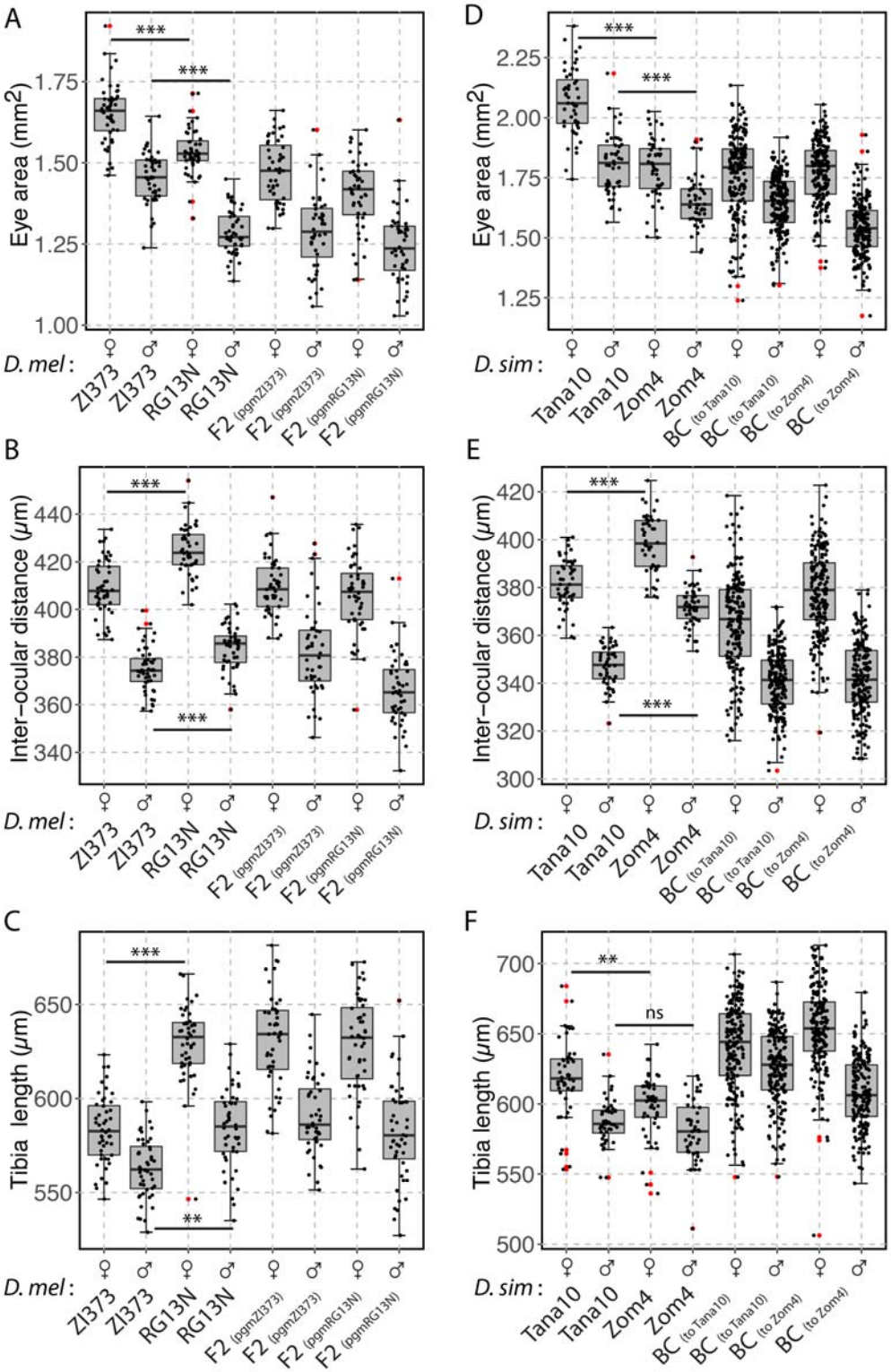

Fig. S4 – Distribution of phenotypes comparing focal strains of *D. melanogaster* and *D. simulans* and their respective QTL mapping populations.

(A) Eye area (mm^2), (B) inter-ocular distance (μm) and (C) posterior tibia length (μm) for

males (n=45) and females (n=45) of the strains ZI373, RG13N and the F2 progeny with either parental grandmother (pgm) (n=96x2). (D) Eye area (mm^2), (E) inter-ocular distance (µm) and (F) T3 tibia length (µm) for males (n=45) and females (n=45) of the strains Tana10, Zom4 (D-E) and backcross to either Tana10 (n=192) or Zom4 (n=192). Statistical comparisons represent t-tests: *** p<0.0001; **p<0.001, ns – p>0.01.

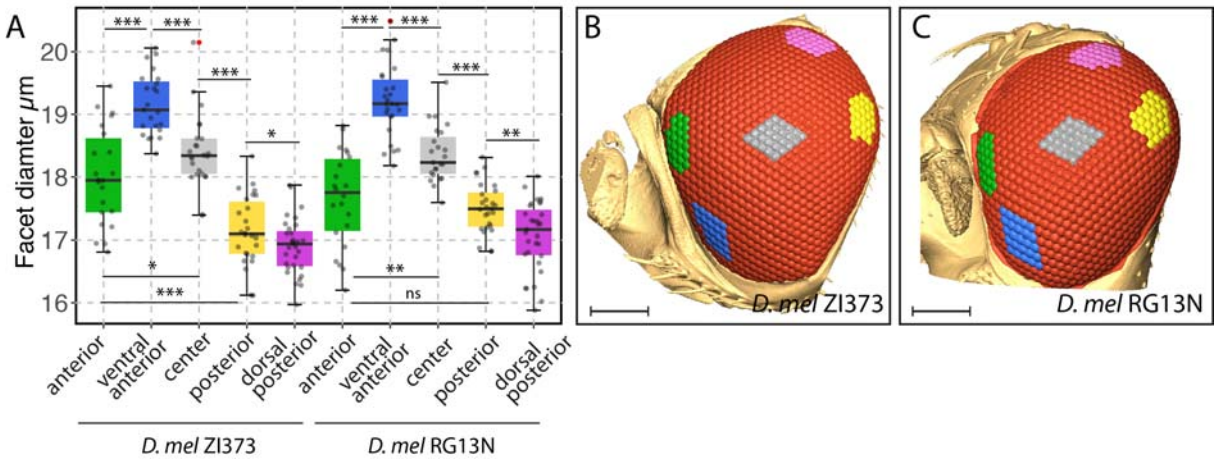

Fig. S5 – Ommatidia sizes across *D. melanogaster* eyes.

(A) Ommatidia facet diameter distribution in clusters selected from the anterior (n=21, ZI373; n=22, RG13N), ventral anterior (n=23, ZI373; n=26, RG13N), central (n=24, ZI373; n=23, RG13N), posterior (n=27, RG13N; n=26, ZI373) and dorsal posterior (n=31, ZI373; n=31, RG13N) of a single female eye from D. melanogaster of the strains ZI373 (B) or RG13N (C). Statistical comparisons represent Tukey's range tests, after considering ommatidial position as a factor in ANOVA: *** p<0.0001; **p<0.001, ns – p>0.01.

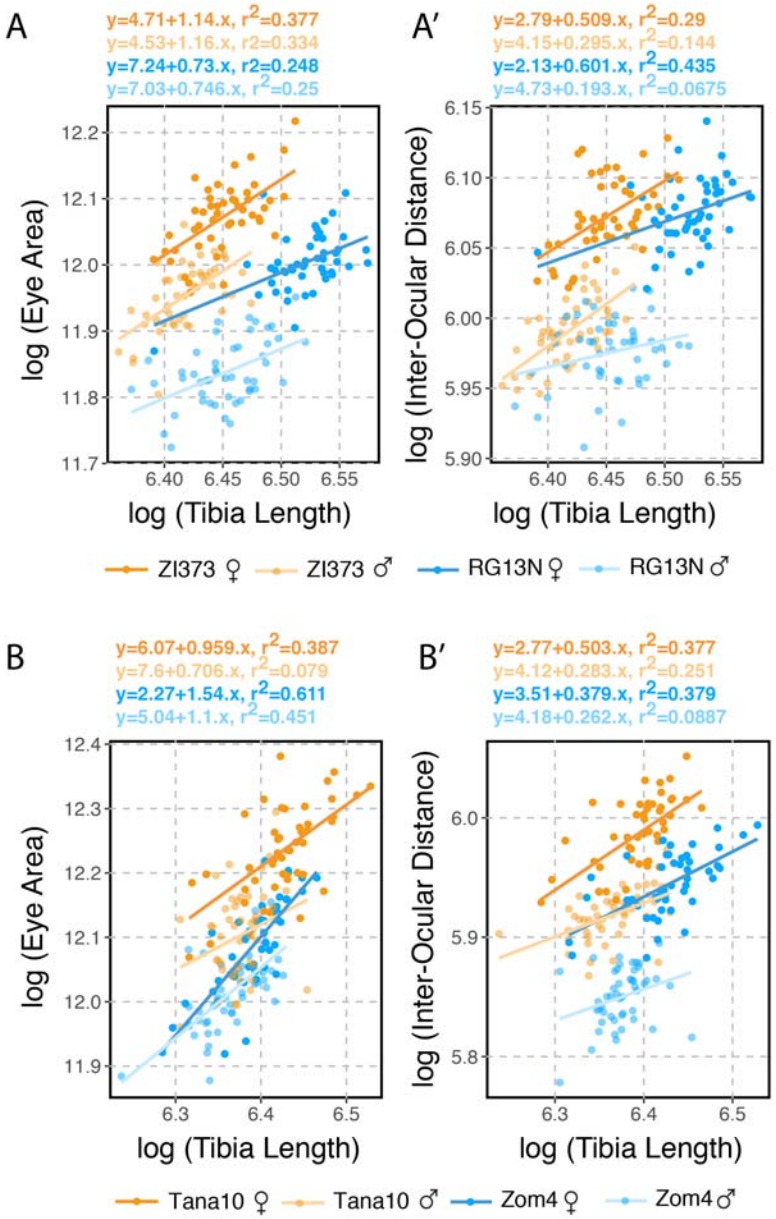

Fig. S6 – **Relationships between eye size and inter-ocular distance with tibia length for the focal strains**

(A) Regression of eye area and (A') inter-ocular distance with the length of the posterior tibia, for males (n=45) and females (n=45) the strains ZI373 (orange) and RG13N (blue) (B) Regression of eye area and (B') inter-ocular distance with the length of the posterior tibia, for males (n=45) and females (n=45) of the strains Tana10 (orange) and Zom4 (blue). Regression equations are indicated above the plots with the same colour as the respective regression line. Lighter coloured lines and points represent male data.

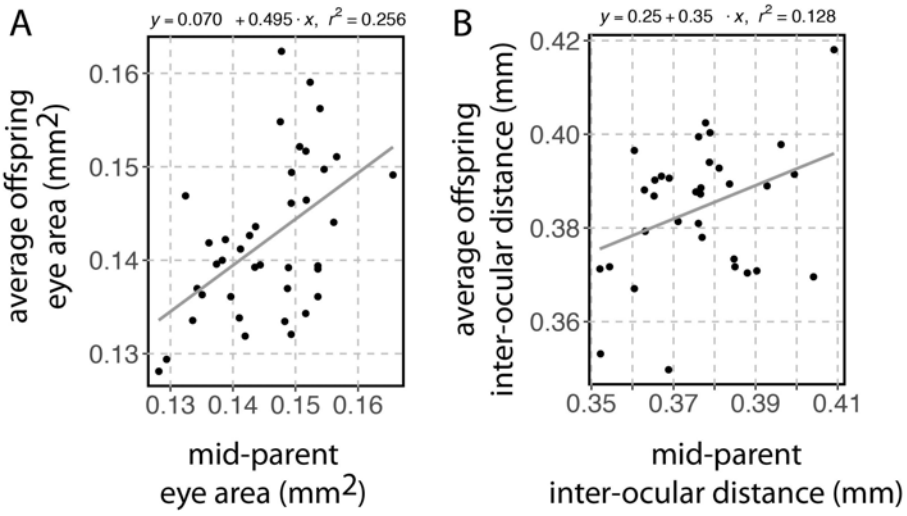

Fig. S7 – Narrow sense heritability (h^2) estimates for eye area and inter-ocular distance.

(A) Regression of average eye area (mm^2) with mid-parent average eye area (mm^2), and (B) regression of average inter-ocular distance (mm) with mid-parent average inter-ocular distance (mm), established from reciprocal crosses between strains (n= 40) of a *D. melanogaster* Zambia (ZI) population. Regression equations are indicated above the respective regression plots.

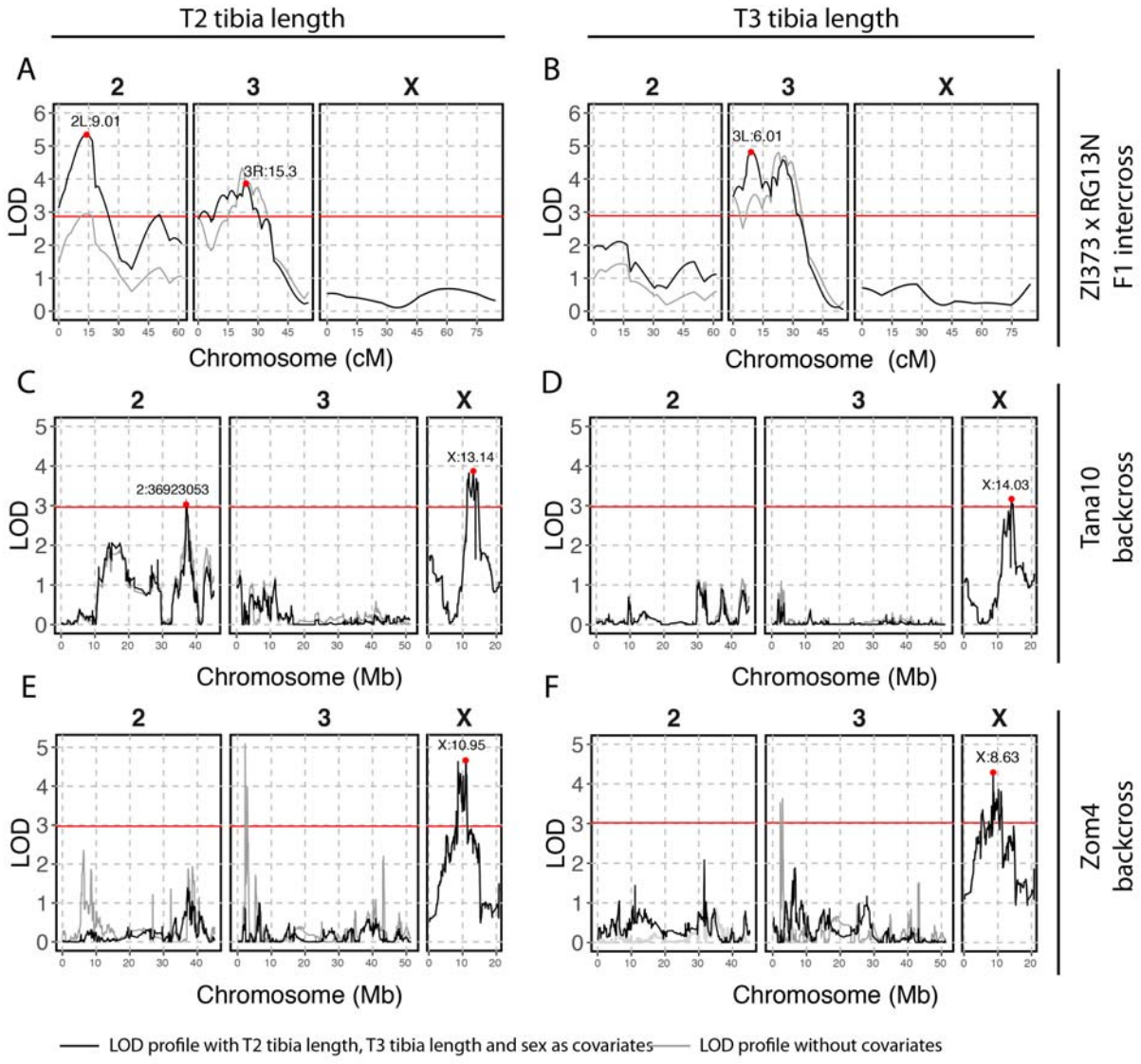

Fig. S8 – **QTL maps following scanone Harley-Knott regression with tibia length.**

(A) T2 and (B) T3 tibia length QTL maps of *D. melanogaster* F2 progeny from reciprocal crosses between strains ZI373 and RG13N (n=192). (A) Middle (Tibia 2) and (B) posterior (Tibia 3) tibia length QTL maps of a *D. simulans* backcross to the strain Tana10 (n=192). (A) T2 and (B) T3 tibia length QTL maps of a *D. simulans* backcross to the strain Zom4 (n=200). A grey line represents LOD profiles without covariates and a black line indicates LOD profiles with sex and the middle and posterior tibia lengths as covariates. A red horizontal line in each plot represents the genome-wide significance LOD threshold of p=0.05. The highest QTL peak above genome-wide significance (p<0.05) for each

chromosome is highlighted as a red dot and their location estimate is indicated above in Mb, according to *Dmel*r.6.45 for *D. melanogaster* and *Dsim*r2.01 for *D. simulans*.